



SRTTU

Journal of Computational and Applied Research  
in Mechanical Engineering

jcarme.sru.ac.ir

JCARME

ISSN: 2228-7922

**Research Paper****Mechanism of surface generation in grinding AA6061-TiB<sub>2</sub>/ZrB<sub>2</sub> in-situ composite****A. Mahamani<sup>a,\*</sup>, S. Jawahar<sup>a</sup> and J. P. Davim<sup>b</sup>**<sup>a</sup>*Sri Venkateswara College of Engineering and Technology(A), Chittoor, India*<sup>b</sup>*Department of Mechanical Engineering, University of Aveiro, Portugal***Article info:****Article history:**

Received: 09/10/2018

Revised: 10/06/2019

Accepted: 13/06/2019

Online: 15/06/2019

**Keywords:**

In-situ composite,

Grinding,

Surface roughness,

Subsurface hardness,

Mechanism.

**\*Corresponding author:**[mahamanisudhan@gmail.com](mailto:mahamanisudhan@gmail.com)**Abstract**

In-situ composites have gained the attention of worldwide researchers in the interest of their greater mechanical properties at the lower reinforcement ratio. Controlling the surface quality of components is a paramount task in the grinding process in order to withstand the creep and fatigue load at service conditions. The current effort is intended to examine the mechanism of surface generation in grinding AA6061-TiB<sub>2</sub>/ZrB<sub>2</sub> in-situ composite under different reinforcement ratios, grinding parameters, and wheel materials. The analysis of results indicates that the grinding of the unreinforced alloy is complicated than the composites. Diamond wheel yields superior performance by generating lesser surface roughness and subsurface hardness at all grinding conditions. Among the various grinding parameters, grinding speed and grinding depth are more sensitive than other parameters. This experimental investigation helps to control the surface roughness and subsurface at various grinding conditions.

**1. Introduction**

Aluminum matrix composites have drawn the attention of many scientists due to their high strength-to-weight ratio, excellent elevated strength, better tribological properties, and corrosion fighting ability when compared to monolithic alloys [1-2]. The aerospace, automotive, space, and defense sectors are consistently seeking weight reduction and enforced to apply the aluminum matrix composites [3-4]. Aluminum matrix composites

manufactured by in-situ route encompass smaller size reinforcements, fine particles, homogeneously distributed reinforcements, uncontaminated matrix-reinforcement interface, improved interfacial strength, and thermodynamically stable in nature [5]. The above listed positive aspects make them attain extraordinary mechanical properties at room and elevated temperatures. TiB<sub>2</sub> and ZrB<sub>2</sub> ceramics possess numerous diverged properties, including high melting temperature, exceptional corrosion resistance, extreme thermal conductivity,

fabulous oxidation resistance, strength, fracture toughness, and admirable creep resistance [6-7]. These reinforcements are chemically stable and act as grain refiner [8]. The addition of the reinforcements into the matrix helps to attain the advantages of both ceramics. Hence,  $TiB_2$  and  $ZrB_2$  ceramics are selected as reinforcements for manufacturing composites. The application of aluminum matrix composite is restricted to aerospace, space, and defense applications where the cost of machining does not bother. However, the commercial applications of the aluminum matrix composites are not appreciated due to the uneconomic machining issue [9]. Surface roughness and sub-surface performance are the unavoidable requirements in the machining process, as they are deemed the manifestation of product quality [10].

Grinding is an inescapable process in the manufacturing industry, and it is used for the final finishing of manufactured component [11-12]. Further, this process is well-advised for machining harder and arduous to cut materials [13-14]. The cutting grit gets worn out at short intervals. However, the worn-out grit has either re-sharpened or cut away at some stage in the grinding process [15-16]. This re-sharpening ability of the grinding wheel makes them to machine harder materials than the grit [17]. During grinding, more specific energy is used up for material removal thereby greater temperature is generated at the grinding zone, in turn, creates the adverse effect like surface alteration, surface defects, and residual stress on the ground surface [18]. Cylindrical grinding is a machining process, which is widely recognized for finishing the components with high degree surface roughness, and to obtain the desired tolerances [19].

The real-time application of the component made by the composites requires a good surface condition. Deviations in the surface condition are highly influenced by fatigue and creep [20-21]. Grindability studies on aluminum matrix composites are widely reported in the literature. Ronald et al. [22] interrogated the consequence of the wheel bond material on grindability of aluminum matrix composites. Electroplated wheel and resin-bonded wheel were selected for the experimental work. Grinding force, surface

roughness, acoustic emission, and temperature were studied as responses. The investigation result indicates that the resin bonded wheel yield better performance than the electroplated wheel. Thiagarajan et al. [23] conducted an experimental investigation on the grindability of Al/SiC composites using cylindrical grinding. The effect of grinding operating parameters including wheel speed, workpiece speed, feed rate, grinding depth, and SiC content on the grinding force, surface roughness, and grinding temperature were examined.

The result obtained from the experimental work indicates that the fine surface roughness and damage-free surfaces are obtained at lower grinding depth, greater wheel, and workpiece speed. Huang and Yu [24] presented an experimental investigation of grinding of Al-SiC composites under dry, wet, cryogenic, and ELID grinding conditions. Result analysis showed that wet grinding offers a lesser grinding force than dry grinding. Huang et al. [25] studied the chip forming mechanism and the shape of chip in grinding of Al-SiC composites with a diamond grinding wheel. They observed different forms of chips, namely matrix chips, reinforcement chips, and matrix-reinforcement chips. More volume of matrix-reinforcement was collected with the shape of chunky and saw-toothed. Lin et al. [26] intended to establish the grindability issues of the AA-7050-6% $TiB_2$  in-situ composite produced by the  $K_2TiF_6$ - $KBF_4$  reaction system.

The influence of grinding operating parameters and grinding wheel materials on grinding force, surface roughness, grinding temperature, and subsurface hardness were investigated. This study resulted that the grinding parameters and wheel materials offer a noteworthy influence on the grinding performance. The material removal mechanism of the grinding process was being as ductile mode, and there was no indication of pull out or fractured particles on the generated surface. Due to very limited attention to grindability issues of in-situ aluminum matrix composites in the literature, the widespread application of the composites in industries is constrained.

In the present study, the composite materials are fabricated by embedding the sub-micron sized

TiB<sub>2</sub> and ZrB<sub>2</sub> at high interfacial strength via in-situ reaction. Mechanism of surface generation in grinding of AA6061-TiB<sub>2</sub>/ZrB<sub>2</sub> in-situ composites under different reinforcement ratio, grinding parameters, and wheel materials requires some understanding for attaining the economic machining rate without negotiating the surface quality. Therefore, an effort is made to establish the mechanism of surface generation in the grinding of the AA6061-TiB<sub>2</sub>/ZrB<sub>2</sub> in-situ composites.

**2. Materials and Method**

AA6061-TiB<sub>2</sub>/ZrB<sub>2</sub> in-situ composites with 0%, 2.5%, 5% and 7.5% reinforcement ratio are used for experimental work. These composites are made by reacting K<sub>2</sub>TiF<sub>6</sub>, KBF<sub>4</sub>, and K<sub>2</sub>ZrF<sub>6</sub> salts. The detailed procedures for synthesizing the composites are presented in the authors' work [27]. Composite samples are solutionized at 505°C for 1 hr followed by aged at 170° C for 6 hr to get homogenization.

The microstructure and XRD sketch of the composite sample is presented in Figs. 1 and 2. Small size (1-2 μm) reinforcement particles, the clean interface between particle and matrix, and homogeneous dispersion of the particle are seen in the Figs. 1 and 2. Al, TiB<sub>2</sub>, and ZrB<sub>2</sub> phases are detected in the XRD pattern. The dimension of the workpiece is Φ30 × 300 mm. Grinding experiments are conducted by using a horizontal spindle cylindrical grinding machine (Heavy duty machine, Indian make).

The photographic view of the experimental setup is illustrated in Fig. 3. Al<sub>2</sub>O<sub>3</sub>, SiC, CBN, and diamond grinding wheels are employed for the experimental work. The surface roughness values are measured using the Mituyoya surface roughness tester (Cutoff length is 5 mm and the evaluation length is 10 mm from the machined edge). Microhardness of subsurface measured by using MH 06 model microvicker hardness tester with 500 gm load. Scanning electron microscopic studies are conducted using a scanning electron microscope (SEM, JEOL6360 LV Model, Karunya University, India). The grinding wheel parameters and ranges of the and grinding parameters are like wheel speed, work

speed, grinding depth, and feed rate are tabulated in Table 1.

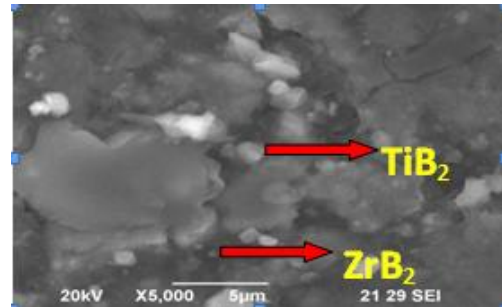


**Fig. 1.** SEM image of 5 % composite sample.

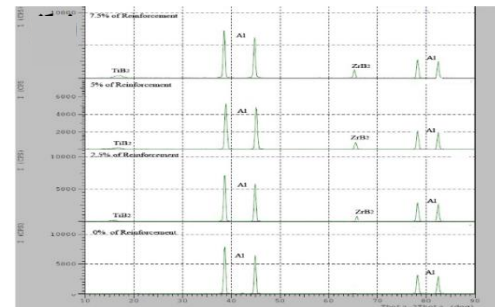


**Fig. 2.** XRD pattern of unreinforced alloy and composites.



**Fig. 3.** Photographic view of the experimental setup.

**Table 1.** The grinding wheel parameters and their levels.

Parameters	Units	Levels		
		Level 1	Level 2	Level 3
Wheel speed	m/s	23.5	33.7	43.9
Work speed	m/min	6	12	26
Grinding depth	μm	10	20	30
Feed rate	m/min	0.06	0.09	0.17
Grinding wheel	Resin bonded diamond, grain size of 80/100, φ300 × 25 mm.			
	Resin bonded CBN, grain size of 80/100, φ300 × 25 mm.			
	Vitrified- bonded Al <sub>2</sub> O <sub>3</sub> , grain size of 80/100, φ300 × 25 mm.			
	Vitrified bonded SiC , grain size of 80/100, φ300 × 25 mm.			

### 3. Results and discussion

#### 3.1. Surface roughness

The effect of wheel speed on surface roughness as a function of wheel materials is presented in Fig. 4(a). This investigation is carried out by fixing the work speed as 12 m/min, grinding depth as 20  $\mu\text{m}$ , feed rate as 0.09 m/min, and 5% reinforcement ratio. It is seen from Fig. 4(a) that the diamond wheel outperforms other wheels in terms of generating very low surface roughness.  $\text{Al}_2\text{O}_3$  wheel generates higher surface roughness for the given experimental conditions.

The surface roughness generated by CBN and SiC wheels is lying between diamond and  $\text{Al}_2\text{O}_3$  wheels. The Knoop hardness number of  $\text{TiB}_2$  is 3370,  $\text{ZrB}_2$  is 1550, SiC is 2480,  $\text{Al}_2\text{O}_3$  is 2100, CBN is 4500, and diamond is 7000.  $\text{TiB}_2$  ceramic has more hardness than SiC and  $\text{Al}_2\text{O}_3$ , and these ceramic phases cause more wear on  $\text{Al}_2\text{O}_3$  and SiC due to rubbing action. As the wheel speed increases the rubbing action on the workpiece also increases.  $\text{Al}_2\text{O}_3$  and SiC wheels are subjected to severe wear. Worn out grinding wheel extends the surface roughness of the ground surface.

The effect of clogging is more on the worn out wheel [28]. Hence, the existence of clogging is also a reason for more surface roughness when using  $\text{Al}_2\text{O}_3$  and SiC wheels. Excessive hardness pertaining to the CBN and diamond wheel causes minimal wear. It is also seen from Fig. 3(a) the enhancement in wheel speed decreases the surface roughness for all wheels. It may be attributed to the enhancement in wheel speed, which reduces the undeformed chip thickness and reduces the contact area between wheel abrasives and work piece [29]. The influence of work speed on surface roughness under a variety of wheel materials is displayed in Fig. 4(b).

This study is conducted by keeping the grinding parameters of wheel speed as 33.7 m/s, grinding depth as 20  $\mu\text{m}$ , feed rate as 0.09 m/min, and 5% reinforced composites. Fig. 4(b) shows that the enhancement in work speed maximizes the surface roughness for all grinding wheels. At higher work speed, the tangential and normal component of grinding force on the surface is maximum [30] The thickness of the undeformed chip is maximized; this phenomenon enhances

the surface roughness. It is obvious from Fig. 3(b) that the surfaces generated by diamond and CBN wheels have lower surface roughness than those generated using  $\text{Al}_2\text{O}_3$  and SiC wheels. The extreme wear resistance of diamond and CBN materials during the grinding process offers lower surface roughness. Variation of surface roughness when increasing the grinding depth under different wheel materials is illustrated in Fig. 4(c).

This investigation is carried out by holding other parameters of wheel speed as 33.7 m/s, work speed as 12 m/min, feed rate 0.09 m/min, and 5% reinforced composites. It is clear from Fig. 4(c) that the increase in depth of grinding hikes the surface roughness despite the consequences of the grinding wheel. The frictions between the workpiece and wheel grain as well as the undeformed chip are relatively more when increasing the grinding depth. This mechanism allows more material removal rate, in turn, increased the surface roughness. The effect of grinding depth offers a very limited impact on the diamond and CBN wheels. Excessive friction at higher grinding depth forms cavities on  $\text{Al}_2\text{O}_3$  and SiC grinding wheel.

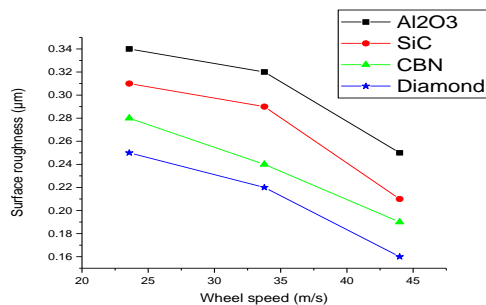
The deposition of the melted chip in the cavities deteriorates the surface roughness. Influence of feed rate on surface roughness under a variety of grinding wheels and parameters as wheel speed of 33.7 m/s, work speed of 12 m/min, and grinding depth of 20  $\mu\text{m}$  is shown in Fig. 4(d). This figure clearly brings out that the enhancement in feed rate increases the surface roughness. This trend is common for all wheels, which are considered for experimental work. These experiments are also conducted by keeping the wheel speed, work speed, grinding depth, and volume content of the composite constant. An increase in feed rate maximizes grinding force alongside the axis of the job rotation, uncut chip thickness, and material removal rate.

A larger material removal rate maximizes the surface roughness. As mentioned earlier, the  $\text{TiB}_2$  and  $\text{ZrB}_2$  are harder ceramics than  $\text{Al}_2\text{O}_3$  and SiC and softer than CBN and diamond. Hence  $\text{Al}_2\text{O}_3$  and SiC wheels allow more particle pulling, whereas diamond and CBN allow cutting off the particles [31]. Hence, the surfaces

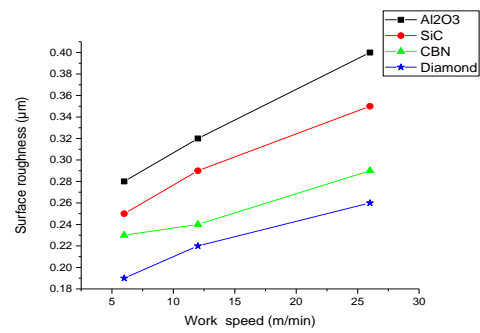
generated by diamond and CBN wheels have lower roughness than other wheels. The influence of reinforcement ratio on surface roughness under various wheel materials is represented in Fig. 4(e). This experimentation is conducted to keep the grinding parameters as wheel speed of 33.7 m/s, work speed of 12 m/min, grinding depth of 20 μm, and feed rate of 0.09 m/min.

Fig. 4(e) represents that the unreinforced alloy has more surface roughness irrespective of wheel materials. It may be attributed to the low hardness of unreinforced alloy exposed to a high temperature environment during grinding. The ductility of the alloy further increases and goes to partial melting. The fused chips attach to the grinding wheel and cause a clogging effect. The deposited chips fasten to the surface and increase the surface roughness. Further, the part of clogged chips with grinding wheel is also deposited on the ground surface and thereby increases surface roughness. It is understandable from Fig. 4(e) that the 2.5% reinforced composites have lower surface roughness than the 7.5% reinforced ones.

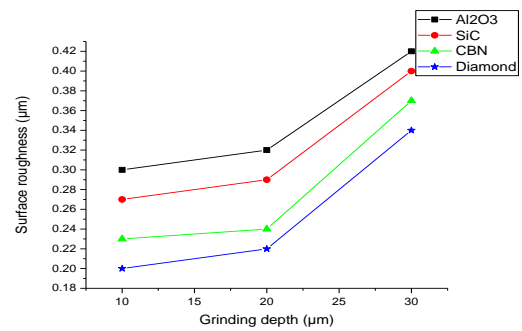
A hike in reinforcement ratio increases the number of particles within the unit area of composites. The presence of excessive volume fractions of the particle increases the surface roughness irrespective of grinding condition and grinding wheel materials. It is also observed from the Fig. 4(e), the surface generated by the diamond and CBN wheels are smoother than those generated using Al<sub>2</sub>O<sub>3</sub> and SiC wheels. Diamond and CBN are considered super ceramics and possess more hardness and wear resistance. These properties enable the cutting through a mechanism while grinding reduces surface roughness.



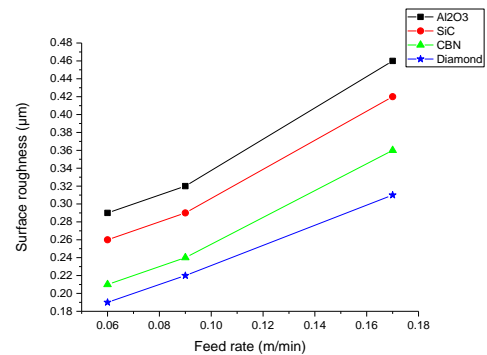
(a) Wheel speed effect



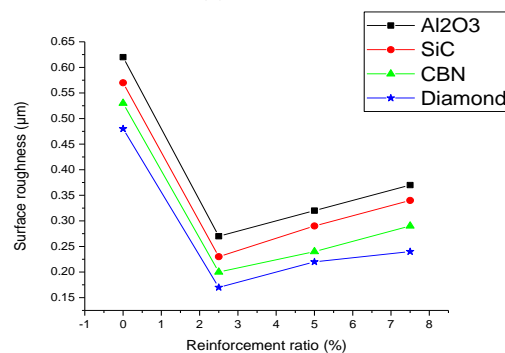
(b) Work speed effect



(c) Grinding depth effect



(d) Feed rate effect



(e) Reinforcement ratio effect

**Fig. 4.** Effect of wheel speed, workspeed, grinding depth, feed rate, and reinforcement ratio on surface roughness.

The clogging effect on diamond and CBN are very negligible due to their high wear resistance. On the contrary, the  $\text{Al}_2\text{O}_3$  and SiC have poor wear resistance. This property allows higher wear rate of the wheel and enhances the clogging effect. The lower hardness wheel permits more particles pulling than cutting through the mechanism. Increased particle pulling effect causes poor surface roughness.

### 3.2. Subsurface hardness

$\text{Al}_2\text{O}_3$  wheel is low cost. A smooth surface can be generated by selecting the appropriate grinding parameters. A diamond wheel is costlier than  $\text{Al}_2\text{O}_3$ . Higher degree surface roughness can be obtained by using the diamond wheel and the wheel damage during grinding is very minimal. Hence,  $\text{Al}_2\text{O}_3$  and diamond wheels are selected for the subsurface hardness analysis.

Fig. 5(a) indicates the microhardness analysis of the subsurface for different reinforcement ratios of the composites. Influence of reinforcements ratio on subsurface hardness is studied by selecting 0%, 5%, and 7.5% reinforced composites and fixing the wheel speed at 33.7 m/s, work speed at 12 m/min, grinding depth at 20  $\mu\text{m}$ , and feed rate at 0.09 m/min. It is clear from Fig. 5(a) that the subsurface hardness of the unreinforced aluminum alloy ground with the  $\text{Al}_2\text{O}_3$  wheel has a higher deviation from the base hardness of the unreinforced alloy. As discussed earlier, under a similar grinding condition, the  $\text{Al}_2\text{O}_3$  wheel causes poor surface roughness due to lower heat dissipation rate, higher worn out, and more clogging effect.

These mechanisms offer more loads and bring more heat to the workpiece. The unreinforced aluminum alloy undergoes partial melting and the ductility of the materials increases. Excessive load and higher ductility facilitate more plastic deformation, in turn, the subsurface hardness is relatively high. At the same grinding condition, the unreinforced alloy ground by the diamond wheel has a lower subsurface hardness. It may be attributed to that the good lubrication, heat dissipation, and minimal clogging effect reduce the subsurface hardness. Fig. 5(a) clearly brings out the comparison of subsurface hardness

developed by  $\text{Al}_2\text{O}_3$  and diamond wheels.  $\text{Al}_2\text{O}_3$  wheel offers more subsurface hardness than the diamond wheel. An increase in reinforcement ratio reduces the grain size of the composites and allow minimum plastic deformation.

The subsurface hardness developed by the  $\text{Al}_2\text{O}_3$  grinding wheel on 7.5 reinforced composites has higher hardness at all points of measurements. The hardness of 7.5% reinforced composite is higher, and the influence of the grinding wheel offer less plastic deformation, and ultimately the subsurface hardness generated by the  $\text{Al}_2\text{O}_3$  wheel is more. On the other hand, the subsurface hardness generated by the diamond wheel is less than the subsurface hardness generated by the  $\text{Al}_2\text{O}_3$  wheel under the same composites and grinding conditions. It may be attributed to the lubrication exhibited by the diamond wheel on the surface, and thereby heat generation is minimized.

This mechanism limits the plastic deformation and reduces the hardness. Similar observations are also made for the 5% reinforced composites.

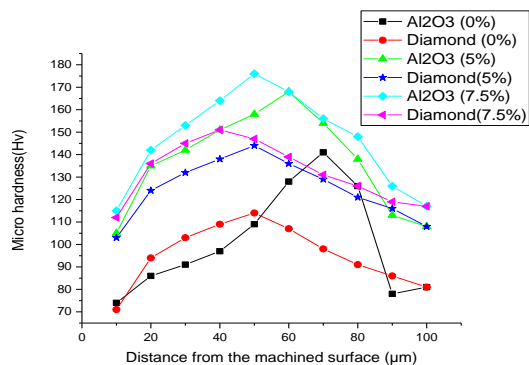
Fig. 5(a) also shows that the increase in reinforcement ratio increases subsurface hardness. However, the plastic deformation phenomenon decreases when the reinforcement ratio rises. Possession of higher hardness at higher reinforcement ratio dominates the mechanism of plastic deformation. This phenomenon allows more subsurface hardness. The influence of wheel speed on subsurface hardness under similar grinding conditions and reinforcement ratio is presented in Fig. 5(b).

The influence of wheel speed on subsurface hardness is studied by selecting the wheel speed of 23.5 m/s and 43.9 m/s by fixing the work speed at 12 m/min, grinding depth at 20  $\mu\text{m}$ , and feed rate at 0.09 m/min. It is evident from Fig. 5(b) that the subsurface hardness generated by the  $\text{Al}_2\text{O}_3$  wheel is higher than that generated by the diamond wheel. Fig. 5(b) also depicts that the increase in wheel speed maximizes the subsurface hardness irrespective of wheel materials. It is due to the higher dissipation of heat on the grinding interface at a higher wheel speed. Excessive plastic deformation on the ground surface maximizes the subsurface hardness. The influence of feed rate on subsurface hardness under different grinding

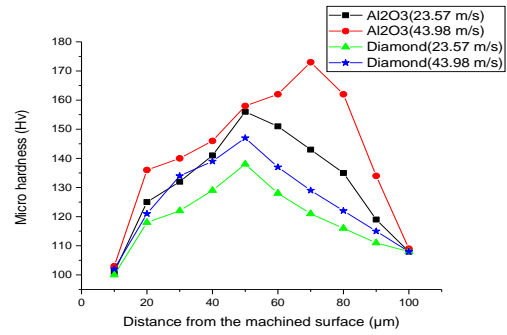
wheels is illustrated in Fig. 5(c). The influence of feed rate on subsurface hardness is studied by selecting the feed rate at 0.06 m/min and 0.12 m/min by fixing the wheel speed at 33.7 m/s, work speed at 12 m/min, and grinding depth at 20  $\mu\text{m}$ .

The subsurface hardness generated by  $\text{Al}_2\text{O}_3$  is higher than that generated by diamond wheels. It is also observed from Fig. 5(c) that the increase in feed rate maximizes the subsurface hardness. It may be attributed to that the higher feed rate enhances cutting effort and maximizes the subsurface hardness. Higher cutting force exhibits more plastic deformation and maximizes subsurface hardness. Fig. 4(d) represents the effect of depth of grinding on subsurface hardness under various grinding wheels. The influence of grinding depth on subsurface hardness is studied by selecting the grinding depth at 10  $\mu\text{m}$  and 30  $\mu\text{m}$  by fixing the wheel speed at 33.7 m/s, work speed at 12 m/min and feed rate at 0.09 m/min. Subsurface hardness generated by  $\text{Al}_2\text{O}_3$  is more when compared to diamond wheels. It is also found from Fig. 5(d) that an increase in grinding depth increases the subsurface hardness.

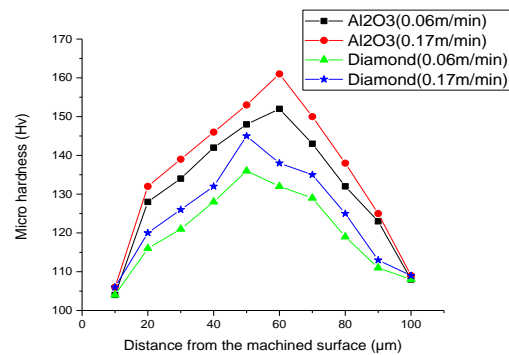
Higher grinding depth maximizes the grinding force normal to the surface and increases the plastically deformed region. The compressive load on the surface enhances the subsurface hardness. The effect of work speed on subsurface hardness as a function of grinding wheel material is displayed in Fig. 5(e). The influence of work speed on subsurface hardness is studied by selecting the work speed at 6 m/min and 26 m/min by fixing the wheel speed at 33.7 m/s, grinding depth at 20  $\mu\text{m}$  and feed rate at 0.09 m/min. It is seen from Fig. 5(e) that diamond wheels are superior to  $\text{Al}_2\text{O}_3$  wheels by exhibiting lower subsurface hardness.



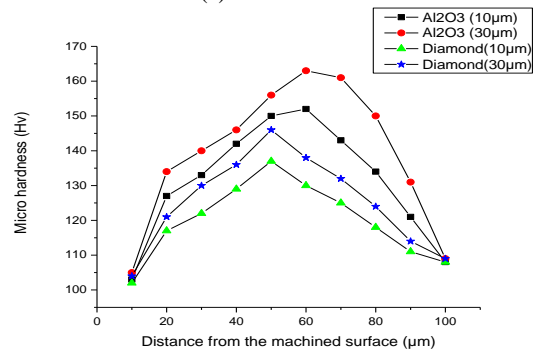
(a) Reinforcement ratio effect



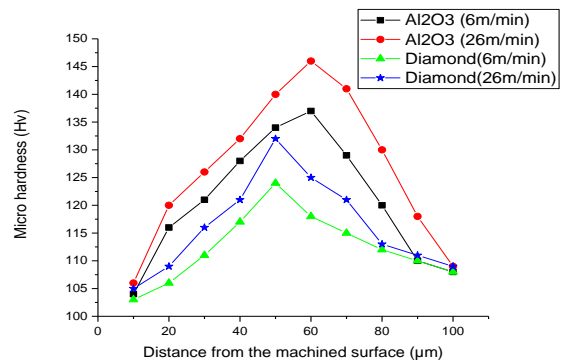
(b) Wheel speed effect



(c) Feed rate effect



(d) Grinding depth effect



(e) Work speed effect

Fig. 5. Effect of reinforcement ratio, wheel speed, grinding depth, feed rate, and work speed on subsurface hardness.

Fig. 5(e) also depicts that the increase in work speed maximizes the subsurface hardness. At higher work speed, the normal and tangential components of grinding force are more, and thereby the depth of plastic zone increases. A wide plastic zone maximizes the subsurface hardness.

### 3.3. Mechanism of surface generation

Understanding the surface generation mechanism in grinding in-situ composites helps to employ the grinding process for economic machining rate without compromising the surface quality. The grit-work piece interaction under various processes parameters and grinding wheels plays a vital role in chip formation and surface generation. A major part of mechanical energy, drawn from the grinding condition, is converted as heat, and a minor part of the energy is spent for the surface generation [33].

Grinding processes have three stages, namely sliding, plowing, and cutting [34]. In the sliding phase, the grit penetration depth is extremely limited and the workpiece is subjected to elastic deformation. The penetration depth is enhanced when the shifting from sliding to plowing phase and allows ridge formation without material removal. Whenever the penetration depth reaches the critical value, the chip formation phase initiates. Grit and work piece interaction determines the cutting processes, tribological characteristics, material pile up, workpiece deformation, and thermo-mechanical system. The number of grains per unit wheel volume and undeformed chip thickness are the major components of the surface generation mechanism [35].

A raise in wheel speed declines the undeformed chip thickness, chip length, the volume of chips, plowing force, shearing force, specific plowing energy, specific shearing energy, and grit- chip contact length [32]. However, friction force and specific total energy are growing up by enhancing the wheel speed. A hike in work speed and feed rate steps up the undeformed chip thickness, chip length, chip volume, plowing force, and shearing force. On the other hand, friction force and specific total energy are drop off when rising the work speed and feed rate. An increment in grinding depth enlarges the uncut chip thickness, length of chips, volume of chips,

and plowing force. Nevertheless, the friction force and specific to the grinding energy decline by enhancing the grinding depth [36]. A swell in wheel speed diminishes the number of grains in the grinding contact zone, whereas an increment in work speed, feed rate, and grinding depth enhances the number of grain in the grinding contact zone.

At higher wheel speed lessens the thickness of the undeformed chip. This mechanism brings more sliding grains and reduces the number of plowing and cutting grains [37]. Grinding depth has greater influence to bring more grain into the contact zone than wheel speed, work speed, and feed rate. A raise in wheel speed reduces the penetration depth, whereas a hike of work speed, feed rate, and grinding depth enhanced the penetration depth. However, the grinding depth is a more influential grinding parameter on penetration depth than the wheel speed, work speed, and feed rate [38].

The thermal expansion of the workpiece due to grinding zone temperature is not reversible when it reaches room temperature. Higher thermal expansion and lower shrinkage of the workpiece under the grinding action provokes the residual stress on the ground surface. Deposition of compressive residual stress on ground surface is advantageous for service conditions, whereas the tensile residual stress brings on fatigue failure [39]. Residual stress with compressive nature is facilitated at higher specific energy grinding conditions. Higher wheel speed, lower wheel speed, feed rate, and grinding depth are favorable conditions to produce residual stress with compressive nature. Excessive wheel speed brings more grinding zone temperature and softens the workpiece, whereas the lower levels of other grinding operating parameters apply mechanical load to the ground surface.

However, ground components may be finished with lower wheel speed and grinding depth. This action enhances the compressive residual stress additionally [40]. Higher wheel speed along with greater grinding depth is a more favorable condition for thermally induced tensile residual stress. Setti et al., [41] correlated these phases with Johnson's Indentation theory. The mode of deformation of indentation is elastic, elastic-plastic, and purely plastic in nature. These modes of deformation are coinciding with sliding, plowing, and cutting zones of grinding. If the

mean contact pressure of the grit is less than 1.1 times of yield strength of the workpiece, the zone comes under elastic deformation. If the mean contact pressure of grit lies between the 1.1 to 2.97 times yield strength of the workpiece, the region is termed as elastic-plastic deformation zone, whereas if the mean contact pressure of grit is greater than the 2.97 times of yield strength of the workpiece, the zone belongs to purely plastic deformation zone.

An increment in reinforcement ratio enhances the yield strength of the composites. For constant grinding, the enhancement in reinforcement ratio raises the mean contact pressure requirement of grit for attaining the purely plastic deformation zone along with chip formation in the grinding process. Further, the insufficient contact pressure of grit facilitates sliding and plowing thereby diminishes the cutting action. The composite material has three regions namely, the matrix, the reinforcement, and the matrix – reinforcement interface. The mean contact pressure necessity for initiating the chip formation of matrix region is fewer than the matrix– reinforcement interface region.

Grit and reinforcement interaction requires more mean contact pressure than the previously mentioned regions. The mechanism of surface generation at the reinforcement region is either particle fracture or particle pulling [42]. Diamond and CBN grits have higher wear resistance. At greater power grinding conditions, these super abrasives are retained their shape with minimal wear against the  $TiB_2$  and  $ZrB_2$  ceramics and assist in better surface quality. In contrast,  $Al_2O_3$  and  $SiC$  grits have poor wear resistance against the  $TiB_2$  and  $ZrB_2$  ceramics and are subjected to more wear. The worn-out grit has a larger negative rake angle with a dual cutting edge and smaller protrusion height. This mechanism brings more sliding action thus spoils the ground surface and induces the residual stress formation.

### 3.4. Surface texture analysis

SEM images of the surface generated by the grinding parameters, i.e., wheel speed of 33.77 m/s, work speed of 12 m/min, grinding depth of 20  $\mu m$ , and feed rate of 0.09 m/min, on 5% reinforced composite using diamond and  $Al_2O_3$  wheel are presented in Figs. 6(a and b). The

figures indicate that the surface generated by the diamond wheel is smoother than that generated by the  $Al_2O_3$  wheel. Fig. 6(a) shows small scratches, ridges, debris, and plastic deformation marks on the ground surface. It may be ascribed that the diamond wheel offers good lubrication, heat conductivity, wear resistance, and a low clogging effect [43].

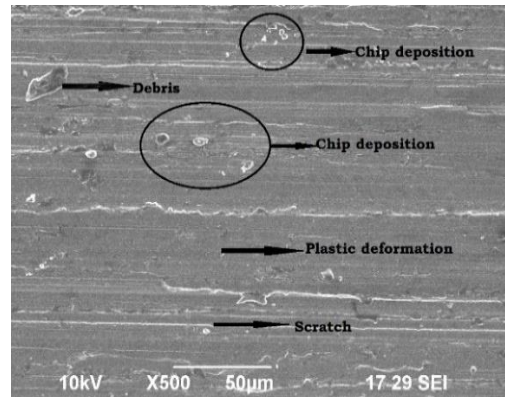
These abilities generate minimal heat at the interface and reduce the load which is subjected to the ground surface. Fig. 6(b) shows excessive debris deposition, thick ridges, and deep grooves on the generated surface. The consequence of grinding load and temperature is that the  $Al_2O_3$  grit loses its shape and the cutting edge is dulled. Worn out grit enhance the sliding and plowing action in turn forms the deep grooves and thick ridges. Figs. 6(c and d) clearly bring out the effect of reinforcements on the surface roughness when grinding with  $Al_2O_3$  wheel is done at the wheel speed of 33.77 m/s, work speed of 12 m/min, grinding depth of 20  $\mu m$ , feed rate of 0.09 m/min on 5% reinforced composites.

Fig. 6(c) indicates that the surface generated on the unreinforced alloy has deep grooves with excessive plastic deformation and the deposition of clogged chips. Low hardness pertaining to the unreinforced alloy allows more wheel clogging effect and severe plastic deformation. Severe deformation due to excessive plowing action and the deposition of clogged chips spoils the surface. In contrast, Fig. 6(d) shows that the surface generated on 5% reinforced composite has minimal scratches and minimum plastic deformation. It is due to the reduced grain size of the composite when increasing the reinforcement ratio. Hence, the hardness and plastic deformation is minimized due to the existence of submicron size reinforcement in the composites.

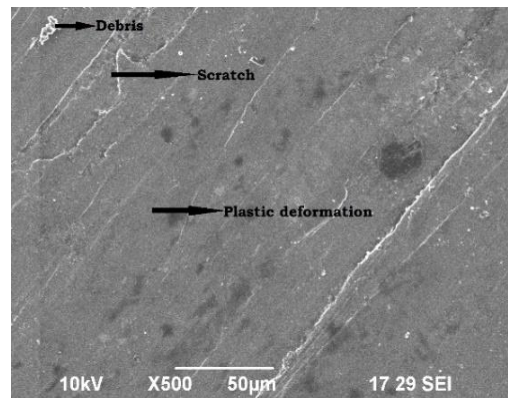
Fig. 6(e) shows the surface generated by wheel speed of 43.9 m/s, work speed of 12 m/min, grinding depth 20  $\mu m$ , feed rate of 0.09 m/min on 5% reinforced composite. Fig. 6(e) exposes that the surface is smooth. At higher wheel speed, the uncut chip thickness is minimum. Hence, the depth of penetration contact reduces, and thereby surface is appeared very smooth. Fig. 6(f) represents the surface produced by wheel speed of 33.77 m/s, work speed of 12 m/min, grinding depth of 20  $\mu m$ , and feed rate of

0.17 m/min on 5% reinforced composite. The influence of higher feed rate on the surface roughness is displayed in Fig. 6(f). The increase in feed rate brings more cutting edges to the grinding zone and the load on the grit increases; therefore, it removes the particles from the composite and forms voids on the ground surface. Further, the influence of plowing action is also observed in Fig. 6(f).

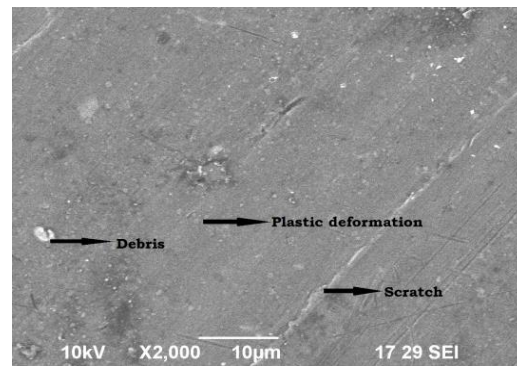
The surface generated by the wheel speed of 33.77 m/s, work speed of 26 m/min, grinding depth of 20 μm, feed rate of 0.09 m/min on 5% reinforced composite is illustrated in Fig. 6(g). Higher work speed induces the smearing effect, ridge and groove formation on the ground surface. These indications are responsible for excessive sliding and plowing action of the grits. Fig. 6(h) exhibits the ground surface generated at the wheel speed of 33.77 m/s, work speed of 12 m/min, grinding depth of 30 μm, feed rate of 0.09 m/min on 5% reinforced composite. Clogging effect, uneven surface, and smearing are noticed in Fig. 6(h). The greater area of contact and cutting action results in excessive surface roughness. Further, Fig. 6(h) clearly brings out the influence of grinding depth on surface roughness than other grinding parameters. Ridge and groove formation on the ground surface indicates that the mode of surface generation is ductile.



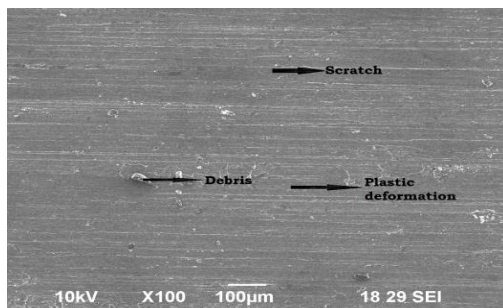
(c) Unreinforced alloy



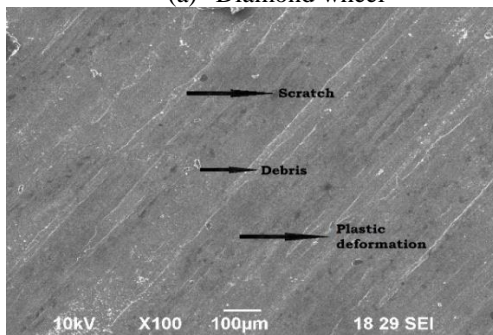
(d) 5 % TiB<sub>2</sub>/ZrB<sub>2</sub> composites



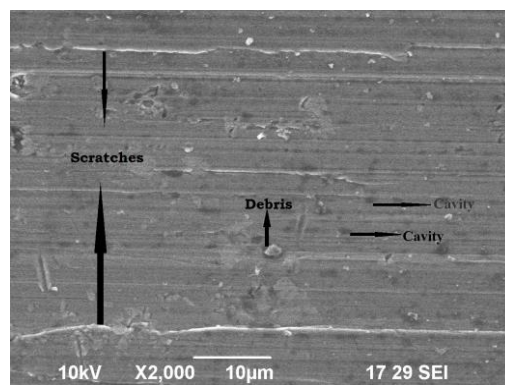
(e) Wheel speed



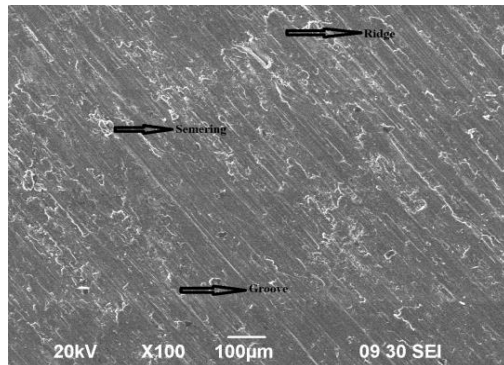
(a) Diamond wheel



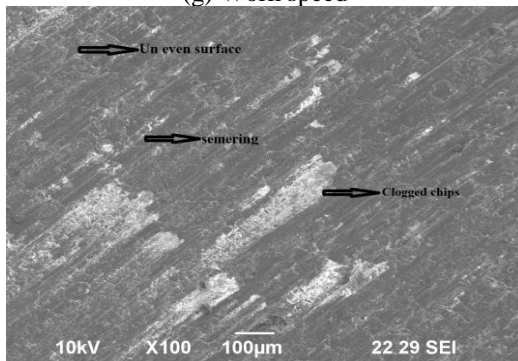
(b) Al<sub>2</sub>O<sub>3</sub> wheel



(f) Feed rate



(g) Work speed



(h) Grinding depth

Fig. 6. (a to h) SEM images of ground surface.

4. Conclusions

The mechanism of surface generation in grinding of AA6061-TiB<sub>2</sub>/ZrB<sub>2</sub> in-situ composites under different reinforcement ratios, grinding parameters, and wheel materials are investigated and the following conclusions are drawn:

1. An enhancement in wheel speed reduces the surface roughness and raises the subsurface hardness.
2. A raise in work speed enhances the surface roughness and subsurface hardness.
3. A hike grinding depth enhances the surface roughness and subsurface hardness.
4. An increment in feed rate hikes the surface roughness and subsurface hardness.
5. An enhancement in reinforcement ratio raises the surface roughness and subsurface hardness; however, the unreinforced alloy has poor grindability due to the clogging effect and excessive plowing action.
6. Diamond wheel is superior to Al<sub>2</sub>O<sub>3</sub> wheel in terms of generating low surface roughness and subsurface hardness. Surface and subsurface

performance of the CBN wheel and SiC wheels lie in between the diamond and Al<sub>2</sub>O<sub>3</sub> wheels.

7. Surface defects like ridge, groove, smearing, void, and fused chip deposition are observed at various grinding conditions; however, ridge and groove formation is observed at all grinding conditions.

8. The mechanism of surface generation is originated by ductile mode. Understanding the surface generation mechanism in grinding in-situ composites benefits employing the grinding process for economic machining rate without negotiating the surface quality.

Acknowledgment

The Authors acknowledge the financial support from Science and Engineering Research Board, DST, New Delhi under Young Scientist Scheme (Ref. No. SB/FTP/ETA-0190/2014).

References

- [1] P. S. Bains, S. S. Sidhu, and H. S. Payal, “Study of magnetic field assisted ED machining of metal matrix composites”, *Mater. Manuf. Process*, Vol. 31, No. 14, pp.1889-1894,(2016).
- [2] S. P. Dwivedi, S. Sharma, and R. K. Mishra, “Characterization of waste eggshells and CaCO<sub>3</sub> reinforced AA2014 green metal matrix composites: A green approach in the synthesis of composites”, *Int. J. Precis. Eng. Manuf.*, Vol. 17, No. 10, pp. 1383-1393, (2016).
- [3] M. K. Surappa, “Aluminium matrix composites: challenges and opportunities”, *Sadhana*, Vol. 28, No. 1, pp. 319–334, (2003).
- [4] J. Myalski, and A. Posmyk, “Processing of sliding hybrid composites with aluminium alloy matrix containing solid lubricants”, *Mater. Manuf. Process.*, Vol. 31, No. 10, pp. 1324-1332, (2016).
- [5] Q. Gao, B. Yang, H. Mei, and H. Wu, “Microstructure and wear resistance of semisolid TiB<sub>2</sub>/7050 composites produced by serpentine tube pouring technique”, *Mater. Manuf. Process*, Vol.31, No. 8, pp. 1029-1894, (2016).

- [6] L. Li, X.T. Wei, G.M. Zheng, L.Y Li, and C.S Dai, "Electroforming of  $TiB_2$  reinforced copper matrix electrode for EDM", *Mater. Manuf. Process.*, Vol. 31, No. 6, pp. 776-780, (2016).
- [7] Z. Amirsardari, M. Salavati-Niasari, R. M. Aghdam, and S. Shakhesi, "Facile carbothermal reduction synthesis of  $ZrB_2$  nanoparticles: The effect of starting precursors", *Mater. Manuf. Process.*, Vol. 31, No. 2, pp. 134-140, (2016).
- [8] Z. R. Yang, H.X. Huan, C.F. Jiang, W.M. Li, X.R. Liu, and S. Lyu, "Evaluation on Dry Sliding Wear Behavior of  $(TiB+TiC)/Ti-6Al-4V$  Matrix Composite", *Int. J. Precis. Eng. Manuf.*, Vol. 18, No. 8, pp. 1139-1146, (2017).
- [9] C. J. Nicholls, B.B. Ian, J. Davies, and M.N. Islam, "Review of Machining Metal Matrix Composites", *Int. J. Adv. Manuf. Technol.*, Vol. 90, No. 9-12, pp. 2429-2441, (2017).
- [10] R. Ferreira, D. Carou, C.H. Lauro, and J.P. Davim, "Surface roughness investigation in the hard turning of steel using ceramic tools", *Mater. Manuf. Process.*, Vol. 31, No. 5, pp. 648-665, (2016).
- [11] Y. Deng, X. Shi, Xiu and M. Liu, "Study on the surface micro-topography in pre-stressed dry grinding process", *Int. J. Abras. Technol.*, Vol. 8, No. 2, pp. 83-96, (2017).
- [12] L. Wan, Z. Deng, T. Liu, H. Tang, and W. Liu, "Experimental investigation of grinding temperature and burn in high speed deep camshaft grinding", *Int. J. Abras. Technol.*, Vol. 7, No. 4, pp. 321 - 336, (2016).
- [13] B. S. Linke, "A review on properties of abrasive grits and grit selection", *Int. J. Abras. Technol.*, Vol. 7, No. 1, pp.46-58, (2015).
- [14] G. Yin, I. D. Marinescu, and M.C. Weismiller, "Grinding force performance with different types of grinding fluids based on a semi-empirical force model", *Int. J. Abras. Technol.*, Vol. 7, No. 3, pp. 167-186, (2016).
- [15] B. Mandal, S. Das, and S. Banerjee, S. "Appropriate application of pneumatic barrier for improving grinding performance", *Int. J. Abras. Technol.*, Vol. 7, No. 1, pp. 26-45, (2015).
- [16] S. Mahata, B. Mandal, J. Mistri, and S. Das, "Effect of fluid concentration using a multi-nozzle on grinding performance", *Int. J. Abras. Technol.*, Vol. 6, No. 4, pp. 257-268, (2014).
- [17] M. Kadivar, A. Zahedi, B. Azarhoushang, and P. Krajnik, "Modelling of the micro-grinding process considering the grinding tool topography", *Int. J. Abras. Technol.*, Vol. 8, No. 2, pp. 157-170, (2017).
- [18] Q. Huang, L. Guo, and I.D Marinescu, "Study on the abrasion mechanism of ultraviolet cured resin bond diamond wheel", *Int. J. Abras. Technol.*, Vol. 7, No. 4, pp. 257-269, (2016).
- [19] A. Zahedi, and B. Azarhoushang, "An analytical force and surface roughness model for cylindrical grinding of brittle materials", *Int. J. Abras. Technol.*, Vol. 8, No. 1, p. 6, (2017).
- [20] D. Pal, A. Bangar, R. Sharma, and A. Yadav, "Optimization of grinding parameters for minimum surface roughness by taguchi parametric optimization technique", *Int. J. Mech. Indus. Eng.*, Vol. 1, No. 3, pp. 2231-6477, (2012).
- [21] K. Song, M. G. Gang, M. B. G., Jun, and B. K. Min, "Cryogenic machining of PDMS fluidic channel using shrinkage compensation and surface roughness control", *Int. J. Precis. Eng. Manuf.*, Vol. 18, No. 12, pp. 1711-1717, (2017).
- [22] B. A. Ronald, L. Vijayaraghavan, and R. Krishnamurthy "Studies on the influence of grinding wheel bond material on the grindability of metal matrix composites", *Mater. Des.*, Vol. 30, No. 3, pp. 679-686, (2009).
- [23] C. Thiagarajan, R. Sivaramkrishnan, and S. Somasundaram, "Cylindrical grinding of SiC particles reinforced aluminum metal matrix composites", *ARPN J. Eng. Appl. Sci.*, Vol. 6, pp. 1819-6608. (2011).

- [24] S. Huang, and X. Yu, "A study of grinding forces of SiCp/Al composites", *The Inter. J. Adv. Manuf. Technol.*, Vol. 94, No. 9–12, pp. 3633–3639, (2017).
- [25] S. Huang, X. Yu, F. Wang, and L. Xu, "A study on chip shape and chip-forming mechanism in grinding of high volume fraction SiC particle reinforced Al-matrix composites", *Int. J. Adv. Manuf. Technol.*, Vol. 80, No. 9, pp.1927-1932, (2015).
- [26] K. Lin, W. Wang, R. Jiang, R. Y. Xiong, and G. Son, "Grindability and Surface Integrity of In- Situ TiB<sub>2</sub> Particle Reinforced Aluminum Matrix Composites", *Int. J. Adv. Manuf. Technol.*, Vol. 88, No. 1-4, pp. 887-898, (2016).
- [27] A. Mahamani, A. Jayasree, K. Mounika, R. K. Prasad, and N. Sakthivelan, "Evaluation of mechanical properties of AA6061-TiB<sub>2</sub>/ZrB<sub>2</sub> in-situ metal matrix composites fabricated by K<sub>2</sub>TiF<sub>6</sub>-KBF<sub>4</sub>-K<sub>2</sub>ZrF<sub>6</sub> reaction system", *Int. J. Microstruct. Mater. Prop.*, Vol. 10, No. 3-4, pp. 185-200, (2015).
- [28] P. Chockalingam, K. Kok, and R. Vijayaram, "Effect of coolant on cutting forces and surface roughness in grinding of CSM GFRP", *Int. J. Indust.Manuf. Eng.*, Vol. 6, No. 8, pp. 1478-1483, (2012).
- [29] D. A. Ilio, and A. A. Paoletti, "Comparison between conventional abrasives and super abrasives in grinding of SiC-Aluminium composites", *Int. J. Mach. Tools Manuf.*, Vol. 40, No. 2, pp. 173–184, (2000).
- [30] P. Li, T. Jin, Z. Guo, J. Yi, and M. Qu, "Analysis on the effects of grinding wheel speed on removal behavior of brittle optical materials", *Proc.11th Int.Manuf. Sci.Eng.Conf. ASME*, (2016).
- [31] C. F. Cheung, K. C. Chan, S. To, and W. B. Lee, "Effect of reinforcement in ultra-precision machining of AA6061/ SiC metal matrix composites", *Scr. Mater.*, Vol. 47, No. 2, pp. 77-82, (2002).
- [32] B. S. Linke, "A review on properties of abrasive grits and grit selection", *Int. J. Abras. Technol.*, Vol. 7, No. 1, pp.46–58, (2015).
- [33] E. Brinksmeier, J.C Aurich, E. Govekar, C. Heinzell, H.W. Hoffmeister, F. Klocke, J. Peters, R. Rentsch, D. J. Stephenson, E.Uhlmann, K. Weinert, and M.Wittmann, "Advances in modeling and simulation of grinding processes", *Ann. CIRP*, Vol. 55 No. 2, pp. 667-696, (2006).
- [34] H. N. Li, T. B. Yu, Z. X. Wang, L. D. Zhu, and W. S. Wang, "Detailed modeling of cutting forces in grinding process considering variable stages of grain-work piece micro interactions", *Int. J. Mech. Sci.*, Vol. 126, pp. 319-339, (2017).
- [35] S. M. Pandit, and G. Sathyanarayanan, "A Model for Surface Grinding Based on Abrasive Geometry and Elasticity", *J. Manuf. Sci. Eng.*, Vol. 104, No. 4, pp. 349-357, (1982).
- [36] B. S. Linke, I. Garretson, F. Torner, and J. Seewig, "Grinding energy modeling based on friction, plowing, and shearing", *J. Manuf. Sci. Eng.*, Vol. 139, No. 12, pp. 1210091-12100911, (2017).
- [37] J. Jiang, P. Ge, and J. Hong, "Study on micro-interacting mechanism modeling in grinding process and ground surface roughness prediction", *Int. J. Adv. Manuf. Technol.*, Vol. 67, No. 5-8, pp. 1035-1052, (2013).
- [38] S. Agarwal, and P. V. Rao, "Predictive modelling of undeformed chip thickness in ceramic grinding", *Int. J. Mach. Tools Manuf.*, Vol. 56, pp. 59-68, (2012).
- [39] K. Salonitis, "On surface grind hardening induced residual stresses", *Proc. CIRP*, Vol. 13, pp. 264-269, (2014).
- [40] E. Heinzl, and N. Bleil, "Using the size effect of specific energy in grinding for work hardening", *Int. J. Manuf. Technol. Manage.*, Vol. 12, No.1-3, pp. 259-269, (2007).
- [41] D. Setti, B. Kirsch, and J. C. Aurich, "An analytical method for prediction of material deformation behavior in grinding using single grit analogy", *Proc. CIRP*, Vol. 58, pp. 263–268, (2017).
- [42] C. Liu, W. Ding, T. Yu, and C. Yang, "Materials removal mechanism in high-speed grinding of particulate reinforced

- titanium matrix composites”, *Prec.Eng.*, Vol. 51, pp. 68-77, (2018).
- [43] N. P. Hung, F. Y. C. Boey, K. A. Khor, Y.S. Phu, and H. F. Lee, “Machinability of aluminium alloys reinforced with silicon carbide particulates”, *J. Mater. Proc. Technol.*, Vol. 56, No. 1-4, pp. 966-977, (1996).

<p>Copyrights ©2021 The author(s). This is an open access article distributed under the terms of the Creative Commons Attribution (CC BY 4.0), which permits unrestricted use, distribution, and reproduction in any medium, as long as the original authors and source are cited. No permission is required from the authors or the publishers.</p>	
--	---

<p><b>How to cite this paper:</b></p> <p>Mahamani Arumugam, S. Jawahar and J. P. Davim, “ Mechanism of surface generation in grinding AA6061-TiB2/ZrB2 in-situ composite”, <i>J. Comput. Appl. Res. Mech. Eng.</i>, Vol. 10, No. 2, pp. 311-324, (2021).</p> <p><b>DOI:</b> 10.22061/jcarme.2019.4224.1511</p> <p><b>URL:</b> <a href="https://jcarme.sru.ac.ir/?_action=showPDF&amp;article=1547">https://jcarme.sru.ac.ir/?_action=showPDF&amp;article=1547</a></p>	
---	--